Tribology International 190 (2023) 109033

Contents lists available at ScienceDirect

Tribology International

journal homepage: www.elsevier.com/locate/triboint

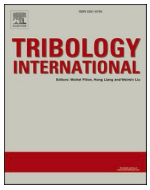

Experimental investigation on the bio-tribocorrosive behavior of Ti6Al4V alloy and 316 L stainless steel in two biological solutions

Alessandro Ruggiero, Marco De Stefano *

Department of Industrial Engineering, University of Salerno, Via Giovanni Paolo II, nr. 132, 84084 Fisciano, Italy

ARTICLE INFO

Keywords:
Tribocorrosion
Biomaterials
Dentistry
Wear

ABSTRACT

In this manuscript the tribocorrosive behavior of two common biomaterials adopted in dentistry such as Titanium Grade V and Steel 316 L was investigated by a tribometer equipped with a three electrodes potentiostat and a confocal interferometric apparatus for a deep worn surface analysis. The experiments underlined that the pH and higher concentration of NaCl induced greater material loss, especially in terms of mechanical-chemical combined action which, estimated by synergistic approach, had a significant impact on the total wear. In addition, Titanium Grade V alloy showed a superior tribocorrosive wear resistance respect to Steel 316 L because of its higher hardness. Lastly, a linear correlation between tribocorrosive current and synergistic factor was found out which could be adopted in future analytical wear models.

1. Introduction

Tribocorrosion can be defined as the phenomenon involving the simultaneous action of tribological effects and electrochemical processes in form of redox reactions, triggered by aggressive external environment, causing the deterioration of the coupled materials [1]. Nowadays, it affects different society sectors such as the marine industry [2], automotive components [3], food processing [4] and, especially, biomedical applications [5] like knee or hip replacements [6] but also dental prosthesis [7], in particular in the interface between abutment and implant [8]. The coexistence of mechanical wear, in all its forms such as adhesive, abrasive, fatigue, etc., and of corrosive wear, in terms of galvanic, pitting, fretting corrosion, cannot be studied separately, since that their synergy could determine an increase in material loss [9]. An example of the latter is the acceleration of corrosive attack originated by the sliding between samples which removes the protective passive layer formed on the surface. On the other hand, the corrosive wear product could act as third body, most of the times hard oxide particles, inducing mechanical abrasion on the counterpart [10]. Unfortunately, the amount of total wear, and the consecutive contact surfaces modifications, has a great influence on the potential loss of functionality of a prothesis [11] or on the microfractures in materials used as medical implants requiring, most of the times, a revision surgery. In that sense, relevant clinical consequences may occur such as the spreading of some metallic ions such as titanium, vanadium, chromium, which are toxic and therefore very dangerous for human cells [12], leading to clinical complications such as severe immune responses, inflammations (*peri-implantitis*) [13] and so on. Unsurprisingly, the common biomaterials like ceramics, metals, polymers, composites [14] are often coupled with specific treatments [15] or coatings having specific anti-wear properties [16]. For instance, Azzi et al. [17] stated that by adding to stainless steel 316 L a SiN_x:H bond layer and diamond-like carbon film, the corrosion and total wear resistance increased, and the friction reduced. Currently, several techniques are available for investigating tribocorrosion [18] such as open circuit potential (OCP), potentiostatic, potentiodynamic, galvanic cell, electrochemical impedance measurements, and so on [19,20], during and in absence of sliding, under free potential or with imposed one. Similarly, the tribocorrosive wear forecast models are, at the moment, object of study [21], both experimental [22] and numerical [23]. In addition, many authors have been carried out different experiments in the last years. As example, Dalmau et al. [24] investigated the relation between current and friction of Ti-Nb-Zr-Ta alloy in phosphate buffered solution. In particular, when current increases, a drop in coefficient of friction was noted. Wang et al. [25] noticed the effect of SiC particle concentration and load applied for Ti-25 Nb-3Mo-3Zr-2Sn alloy in Ringer's solution, finding out that the wear increased if the particle concentration was higher, and the applied load was lower. The porosity, instead, was investigated by Shivaram et al. [26] for Ti–20 Nb–5Ag in simulated body fluid noting that it has a positive role in tribocorrosion response. Even from a biological point of view, because the bone can

* Corresponding author.
E-mail address: mardestefano@unisa.it (M. De Stefano).

https://doi.org/10.1016/j.triboint.2023.109033
Received 26 July 2023; Received in revised form 6 September 2023; Accepted 20 October 2023
Available online 22 October 2023

grow inside the micropores providing major stability. Royhman et al. [27] compared the mechanical performance of Titanium Grade V with CoCrMo alloy in synovial fluid as temporomandibular implants, noting that the second one had better anti-corrosive wear properties. However, the choice of biomaterial is not a trivial task because it should take in consideration not only the mechanical but also the topographical variables such as roughness which, as demonstrated by Sivakumar et al. [28], is strictly correlated with the corrosion resistance and total wear. On the other hand, even the biological and chemical properties like biocompatibility and bioactivity are relevant for a long-term survival of the prothesis. Moreover, Neto and Rainforth [29] evaluated, for four type of titanium alloys, immersed in a new-born calf serum, the impact of potential and microstructure on total wear. The outcomes showed the abrasion as dominant mechanism and the formation of graphite tribofilms and denatured proteins. Wang et al. [30] analyzed the impact of proteins on CoCrMo alloy which determined more deformation influencing, at the same time, the microstructure of the sample. The latter induces also diverse material response as indicated by Carquigny et al. [31] comparing the tribocorrosive behavior of stainless steel 316 L, Titanium Grade V and Ti–10Zr–10 Nb–5Ta alloys noting better anti-wear performance of titanium samples in all solutions with the exception of the ones including the proteins. Consequently, the constituents of the biological fluid play a significant role in the tribocorrosive behavior, in terms of ion release and passive film formed, of the samples, as stated by Yan et al. [32] concerning the structure of bovine serum. The normal load, instead, was evaluated by Axente et al. [33] for stainless steel 304 L in biological Hank medium: more volume loss was appreciated when the force increases. On the contrary, Yazdi et al. [34] for Titanium Grade V immersed in phosphate buffered saline solution, found out that the specific wear rate for unit of force decreased when the load increased as result of a higher coverage of the tribofilms. Hence, a general law, capable of correlating all the factors impacting on the phenomenon, has not been achieved yet. The main complication is the great number of variables involved [35] from different engineering areas: the chemical as pH and solution chemical composition; the mechanical with hardness and Young's modulus; the physical as density, temperature; the tribological as coefficient of friction, the forces exchanged and etc.

This manuscript, thus, provides an attempt to better understand this phenomenon in different ways: analyzing the material response, figuring out the relevance of determined variables and trying to find out probable correlations which provide the basis for the construction of analytical models. More in detail, two biomaterials were chosen: stainless steel 316 L and Titanium Grade V, which are commonly adopted in implantology as dental prosthesis material [36,37]. Their mechanical and chemical response was investigated in the two biological solutions as Ringer and physiological one and discussed from a tribological point of view. The current, potential, friction trends and the total wear contributes, calculated by the synergistic approach, were presented and discussed.

2. Materials and methods

The samples, object of investigation, were stainless steel 316 L and Titanium Grade V alloy of mechanical and chemical properties reported in Table 1. The compositions by weight of the specimens were respectively:

1. 63.145% Fe, 18% Cr, 14% Ni, 2% Mn, 2% Mo, 0.75% Si, 0.045% P, 0.03% S, 0.03% C
2. 90% Ti, 4% V, 6% Al

Table 1
Mechanical and chemical properties of samples investigated.

Material	Density ρ [g/cm^3]	Hardness H [MPa]	Molecular weight MM [g/mol]	Young's modulus E [MPa]	Poisson's coefficient ν []
Steel 316 L	7.70	2255	56.11	206′000	0.33
Titanium Grade V	4.42	3884	46.75	110′000	0.32

Ringer's solution (pH=7.3)

The geometries of the contact bodies are cylindrical of diameter 25 mm and height 6 mm; each one presents a value of arithmetical surface roughness of 0.70±0.5 μm. They were coupled with Titanium Grade V sphere (Fig. 1) of diameter 6 mm (R_a=0.6 μm), providing a mean Hertzian pressure of 548 and 458 MPa and a maximum Hertzian pressures respectively equals to 822 and 687 MPa. This range of pressure outlines the stress regime of the coupling implant-abutment of a common dental implant [38]. The specimens were immersed in two biological solutions as Ringer's and physiological one of compositions reported in Tables 2–3. Finally, before the tests, the samples were cleaned from all the potential impurities in ethanol bath and subsequently dried off.

The experiments were carried out by a Ducom POD-4.0 modular reciprocating tribometer and Ivium potentiostat with three electrodes (Fig. 2), both equipped by own software for output processing. The working electrode (WE) is connected by a metallic frame with the sample, whereas the counter electrode (CE) is in graphite and the reference (RE) in silver chloride (AgCl/saturated KCl, E = 0.197 V). Finally, the pin holder and the cup are in polyethylene since it is electrically insulating.

2.1. Techniques of investigation

First of all, the tests were conducted at environmental temperature (22±1 °C). The open-circuit potential tests for the four couplings were

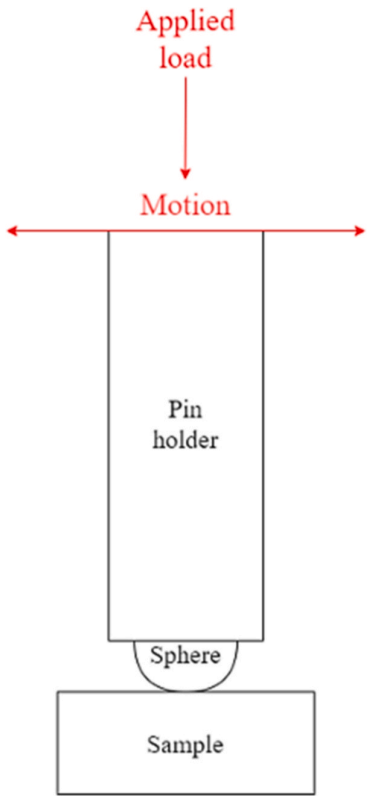

Fig. 1. Schematical representation of the tribological coupling.

Table 2
Chemical composition of Ringer's solution.

Compositions	Quantity [g] for 1 L of solution
Sodium chloride-NaCl	9
Calcium chloride dihydrate-$CaCl_2x2H_2O$	0.24
Potassium chloride-KCl	0.43
Sodium bicarbonate-$NaHCO_3$	0.2
Water-H_2O	990.13

Physiological solution (pH=7.5).

Table 3
Chemical composition of Physiological solution.

Compositions	Quantity [g] for 1 L of solution
Sodium chloride-NaCl	3
Water-H_2O	997

achieved when the OCP potential changes of less than 50 mV per half an hour [39], requiring an interval of time variable in the range 1–3 h according to the sample type. During this phase, an oxide passive layer is formed on the contact surface, in accordance with the chemical reaction described in Eq. (1):

$$M + nH_2O \rightarrow MO_n + 2nH^+ + 2ne^- \quad (1)$$

Where M is the general corroded metal, the water as the corresponding fluid medium, n the number of exchanged electrons and MO_n the oxide layer.

After that, the potentiodynamic curves were extrapolated by starting at − 0.1 V under the OCP imposed and increased up to + 0.1 V over OCP with a scan rate 0.1 mV/s. Concerning the tribocorrosion, the tribometers was set up with the following input parameters: frequency 2 Hz, stroke length 5 mm, normal load 4 N, for a duration of exactly 1 h but divided in three phases reported just below.

1. 20 min without sliding for OCP stabilization
2. 20 min of sliding with no imposed potential and current to control the synergistic effect of wear and corrosion. A total of 2400 cycles were performed simulating a daily masticatory activity [40]
3. 20 min with no sliding to monitor of OCP in static conditions after the impact of tribocorrosive wear

In addition, potentiostatic tests with OCP imposed were carried out with aim of monitoring the current trend during sliding between the bodies and of comparing this value to that with no movement between surfaces obtained by potentiodynamic technique. The test lasted, in this case, 15 min divided in one phase of 300 s with no sliding, 300 s with sliding where an average current was calculated, and final 300 s with no motion.

Lastly, all the tests were carried out three times for achieving repeatability of the results.

2.2. Wear model

The total wear (W) was estimated by synergistic approach [41] as indicated in Eq. (2). The mechanical wear (M) was achieved by the classical Archard's Eq. (3) carrying out a dry tribological test of 20 min for the calculation of wear constants, with the same input conditions presented previously. On the other side, the chemical part (C) was calculated by Faraday's law (4). The synergy (S), finally, as subtraction of these two terms from the total.

$$W = M + C + S \quad (2)$$

$$M = \frac{K}{H} \cdot N \cdot s \quad (3)$$

In (3), K is Archard's constant (reported for both the investigated tribosystems in Table 4); their value were comparable with the ones presented in literature [42], N is the normal load, H the hardness and s the total sliding, which resulted equals to the frequency x stroke length x 2 x testing time.

$$C = \frac{I \cdot MM \cdot t}{n \cdot F \cdot \rho} \quad (4)$$

In (4), I is the current obtained by potentiodynamic curves [39], MM is the molecular weight, t the testing time, n the number of electrons exchanged in the tribosystem, equals to 2 for the stainless steel 316 L and 4 for titanium alloy [43], F the Faraday constant equals to 96, 485 C/mol and ρ the density. Subsequently, the topography of the samples was deeply investigated via optical confocal laser microscope capable of conducting confocal technique or interferometry techniques, equipped with lens of 5x-20x and 50x of magnification. The tool owns a damping table to cutoff potential external vibrations and Sensofar software to process the measured data. The total wear was estimated both by subtracting the post-test profile from the original one and by

Table 4
Archard's constants of the samples analyzed.

Material	Archard's constant
Steel 316 L	$1.01 * 10^{-4}$
Titanium Grade V	$7.72 * 10^{-5}$

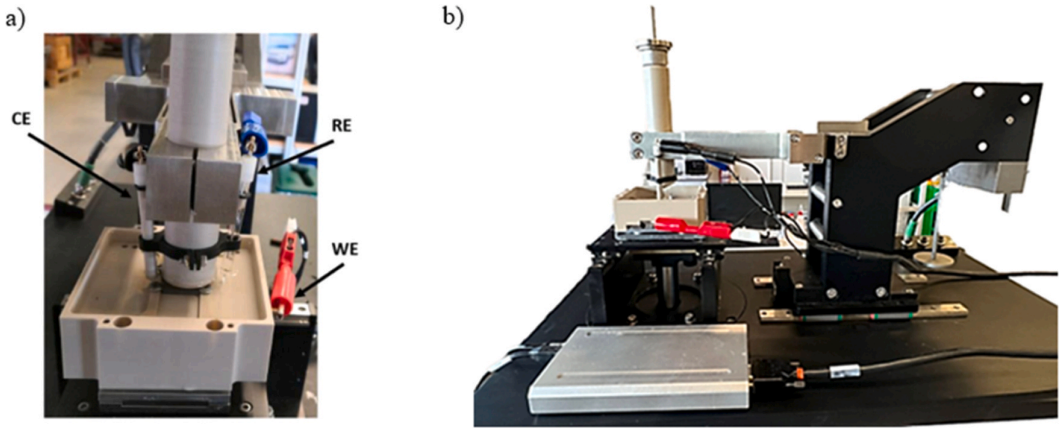

Fig. 2. In-situ machine setup for tribocorrosion test: lateral view with the three electrodes (a) and frontal view with the potentiostat connected.

weighing method through a scale of sensitivity of 0.1 mg. The entire procedure for the estimation of tribocorrosive wear is summarized in the flow chart reported in Fig. 3: after the definition of mechanical and chemical properties of specimens and solution, pre-test topographical characterization was carried out. Successively, the five techniques discussed were performed providing the factors required by the synergistic approach. At the end, the post-test surface characterization was achieved, and the total wear calculated.

3. Results and discussion

In a first phase, each sample was tested in absence of sliding and under free potential, in order to evaluate the open circuit potential for the two solutions. The stabilization phase provides OCP values (vs AgCl/

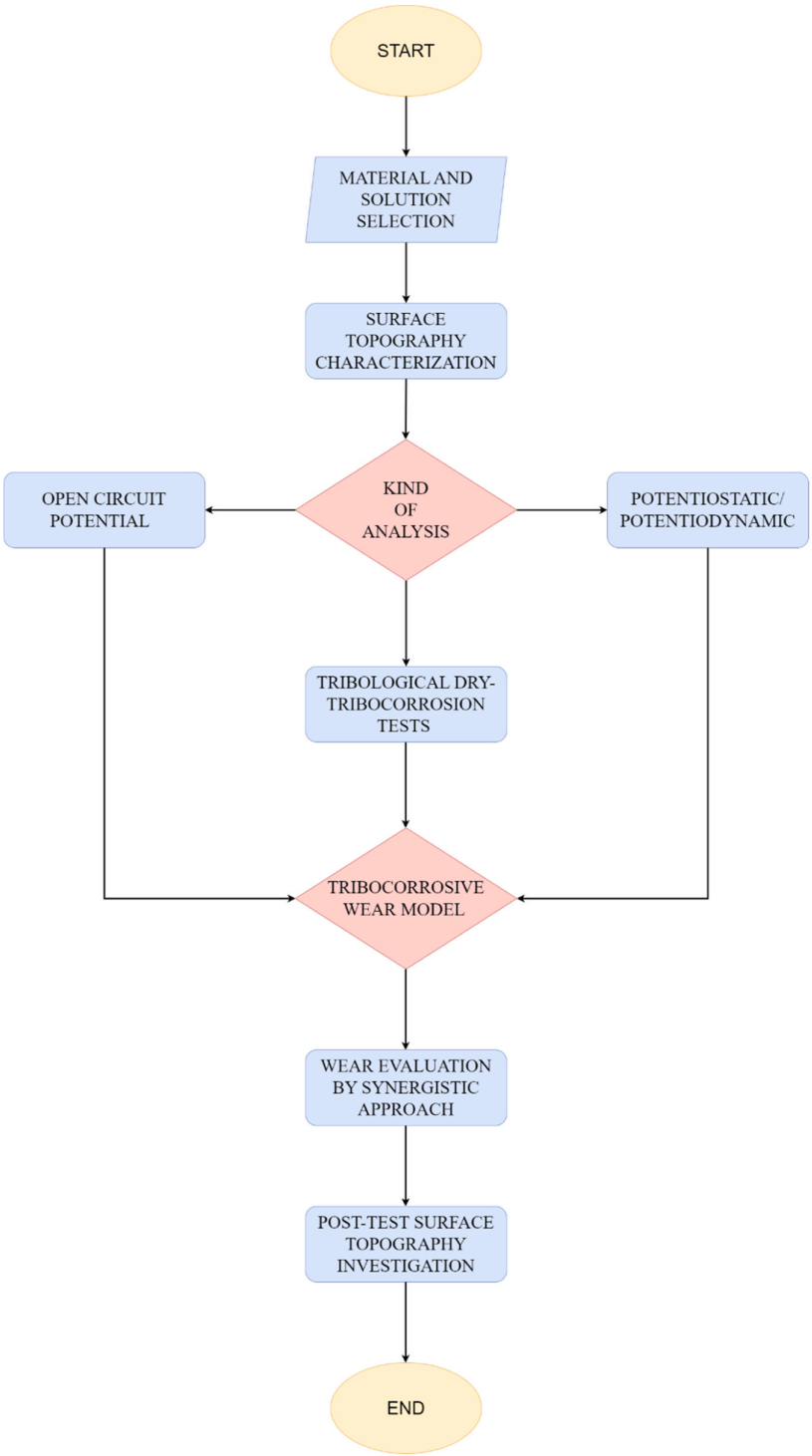

Fig. 3. Flow chart of tribocorrosive wear evaluation.

saturated KCl) respectively for stainless steel 316 L and Titanium Grade V, of − 2.70±0.14, − 25.04±1.25 mV, for Ringer's solution and of − 33.60±1.68 and + 24.68±1.23 mV, for the physiological one. After that, the samples were subjected to the potentiodynamic tests in accordance with the input conditions introduced previously. The curves *E-log I* can be appreciated in Fig. 4, highlighting the diverse response of the two samples for Ringer's solution (Fig. 4a) and for physiological one (Fig. 4b), whereas in Table 5 the values of the current and polarization resistance extrapolated from the curves are reported. The range of potential imposed plays a key role in corrosive behavior modelling of real biological applications because simulating the change of the chemical composition of human saliva, as result of food habits, or of the chemical components of synovial fluid. In addition, it is possible to estimate the chemical behavior of the materials without any mechanical damage [44].

As it easily observable the corrosive behavior of the samples is different due to the chemical nature of the medium. Indeed, the Ringer's one is more corrosive than the physiological owing to the higher concentration of NaCl [45,46] and to the slightly lower pH [47,48]. In particular, the current becomes even 10–30 times higher whereas the polarization resistance 6 times greater by switching the two solutions as prove of the relevance of its chemical structure. Moreover, focusing on the material, it was found that titanium had the worst performance compared with the stainless steel in both the solutions, because of the formation of less tough protective oxide layer. Moreover, the stainless steel owns chemical elements such as chromium and molybdenum which help alloys to contrast the corrosive effect. In any case the current range is of the order of 10^{-7}-10^{-9}A and the polarization resistance of 10^{4}-10^{5} Ω which are extremely small values but, at the same time, reasonable both considering the resistance to corrosion of these samples in these biological fluids and that the solutions are essentially not acid simulating normal conditions [49]. Secondly, the tribocorrosion tests were conducted providing the trends shown in the next graphs for stainless steel 316 L (Fig. 5a) and Titanium Grade V (Fig. 5b). After 20 min where the potential is completely stabilized, the sliding starts with a foreseeable decrease as a consequence of the rupture of the initial oxide layer which subjects the sample to the synergistic action of corrosion and wear. During the motion, the fluctuations can be interpreted as the rupture and the successive formation of the protective layer with no possibility of total recovery [50] because of the plastic deformation induced by the wear. Finally, when the motion is stopped, it increases again, as expected, because of the repassivation [51], almost reaching its initial value [52] with maximum discrepancy, respect to the starting one, equals to 8 mV for Titanium Grade V in Ringer's medium. More precisely, the stainless steel 316 L provided a final potential of − 7.5±0.38 mV and − 38.86±0.9 mV respectively for Ringer's and physiological solution. On the contrary, Titanium Grade V respectively − 33±1.25 mV and 23.35±1.17 mV. The maximum drop during the motion, was, instead, 20.24±1.01 mV and 43.16±2.18 mV respectively for Steel 316 L and Titanium Grade V in Ringer's medium, 16.30±0.82 mV and 30.01±1.5 mV in physiological one. The highest discrepancies are referred to titanium sample in both solutions confirming again the formation of less hard passive layer.

Table 5
Current and polarization resistance values of the two samples for both solutions extrapolated by the potentiodynamic curves.

Material \solution	Ringer		Physiological	
	I_{corr} [μA]	R_p [Ω]	I_{corr} [μA]	R_p [Ω]
Steel 316 L	0.12±0.006	1.50±0.08 * 10^4	0.004±0.001	1.01±0.15 * 10^5
Titanium Grade V	0.26±0.013	1.13±0.06 * 10^4	0.025±0.003	6.74±0.34 * 10^4

From a tribological point of view, instead, the trend of friction coefficient (Fig. 6) was estimated during a tribocorrosion test at no potential conditions [53] for 1200 s. After a rapid rise with the sliding inception as a result of the removal of the protective layer, the COF evolution is characterized by several oscillations emerged from the rupture of oxide and wear debris [54], followed by a progressive decrease. It is reasonable to suppose that both the oxide and the bare material particles are not completely ejected from the sliding track, probably because the number of particles removed, which is influenced by the normal load [55], is lower than ones formed during the motion [56], acting, therefore, as protective third bodies against the tribochemical attack of the tribosystem. In Fig. 7, the mean values of friction coefficient are indicated in order to compare the different response of the materials object of investigation. The outcomes underline the absence of a complete fluid lubrication for all the couplings where the dominant kind is the mixed one, except for the Titanium Grade V immersed in physiological solution which presented a fluid film lubrication. Moreover, the highest values are reached by steel 316 L

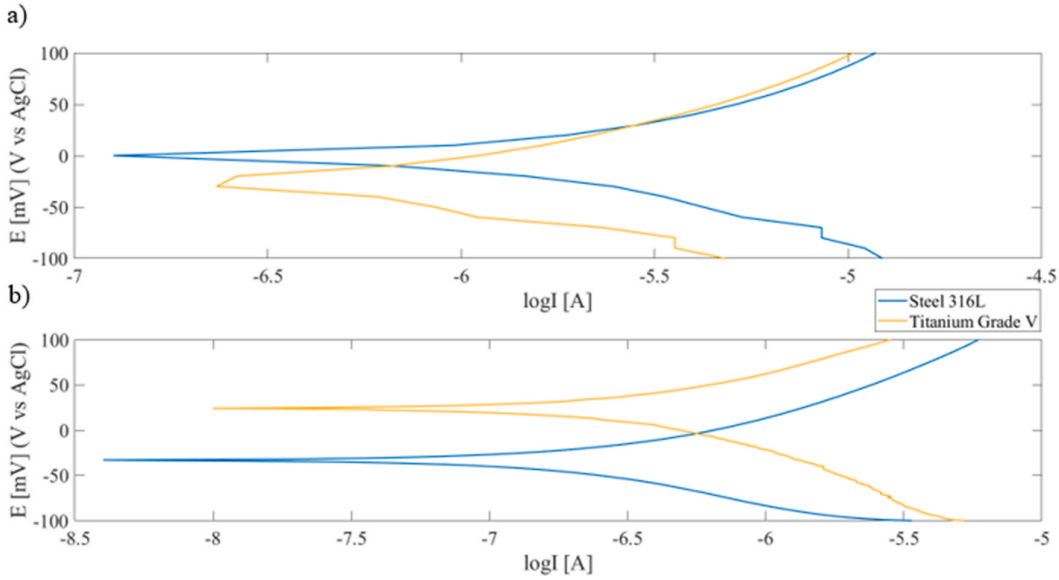

Fig. 4. Potentiodynamic curves of the two samples for Ringer (a) and physiological (b) solution.

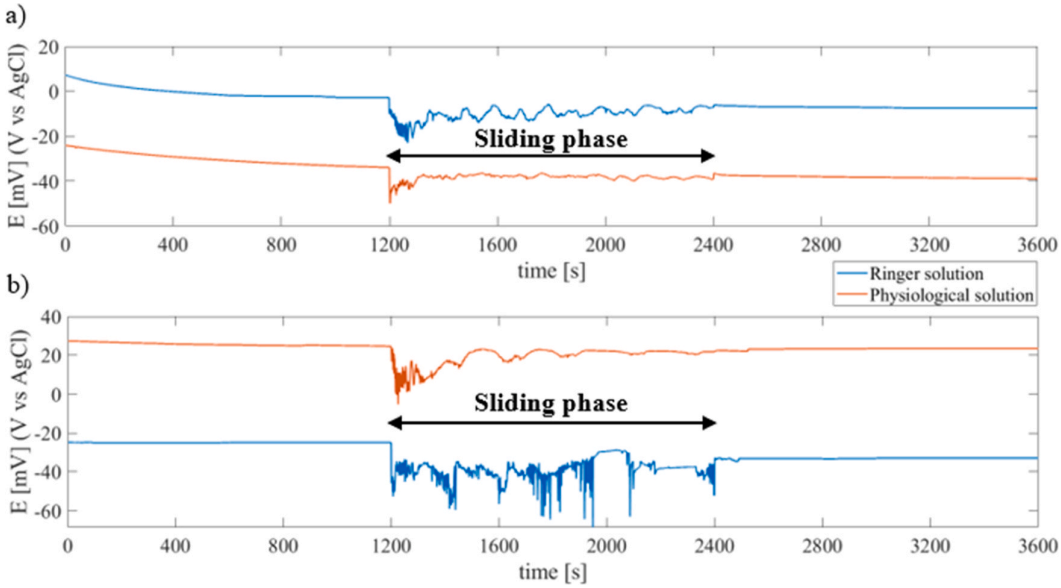

Fig. 5. OCP trend during the tribocorrosion test for Steel 316 L (a) and Titanium Grade V (b) immersed in Ringer and physiological solutions.

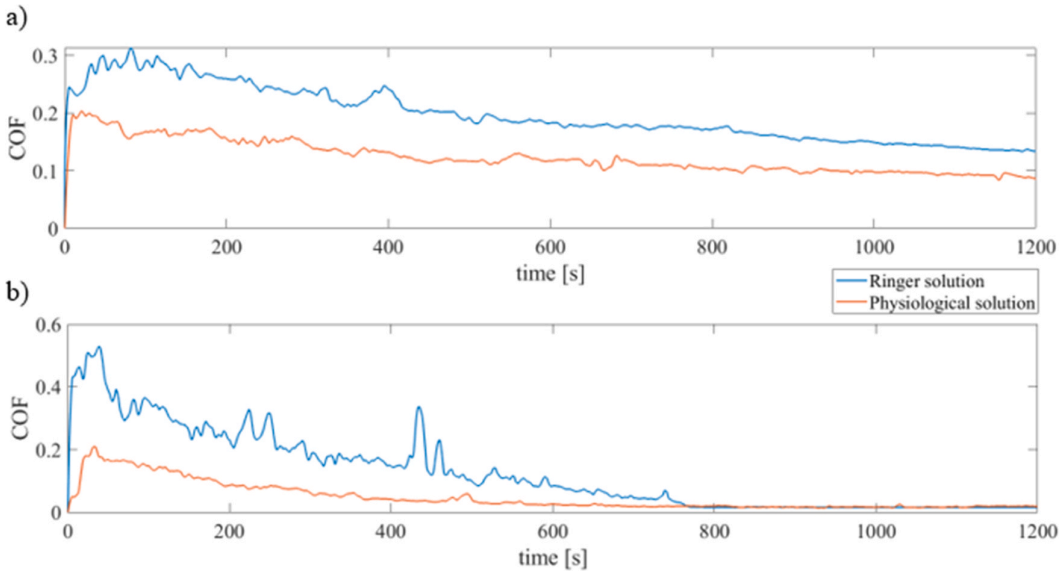

Fig. 6. Coefficient of friction evolution during a tribocorrosion test for Steel 316 L (a) and Titanium Grade V (b) for the two solutions.

followed by titanium alloy, proportionally to the decrease of hardness, for both solutions. On the other hand, also the chemical aspect has its importance as showed by the graphs where a significant decrease, for both the samples, is noted when the solution is changed. The results highlights, thus, the multidisciplinary of tribocorrosion phenomenon as well as the synergistic action of both mechanical and chemical properties. This will be confirmed successively when the analysis of the current during a tribocorrosion test will be presented, demonstrating a massive increase of this variable respect to the potentiodynamic case [57].

3.1. Wear estimation

The different wear tracks, obtained after the tests, are exposed in Fig. 8 whereas the total estimation of material loss, calculated after the tribocorrosion experiments, is reported in Fig. 12. The track is almost evident only for stainless steel 316 L and titanium alloy in Ringer's medium with average depth of 25 μm and 5 μm highlighting again the more aggressivity of the first medium. On the other hand, since in sliding wear the performance of the entire tribosystem counts, also the wear response of counterpart was analyzed founding out that the titanium sphere was only partially worn. For instance, the maximum was referred to the stainless steel 316 L in Ringer solution where the wear was estimated equals to $8 \bullet 10^{-4} \pm 0.03$ mm^3 ($8.33 \bullet 10^{-6}$ mm^3/Nm) and, thus, more than two order of magnitude lower than the specimen. Similar results were noted for the other couplings. Concerning, instead, the main mechanism of material loss, the investigation was carried out adopting a lens of 50x of magnification and the software MountainsLab Premium 9. Arithmetical roughness values changes were found out in all the couplings, but more pronounced for Ringer's medium, as result of wear action. In particular, as reported in Fig. 9, a particle analysis applying

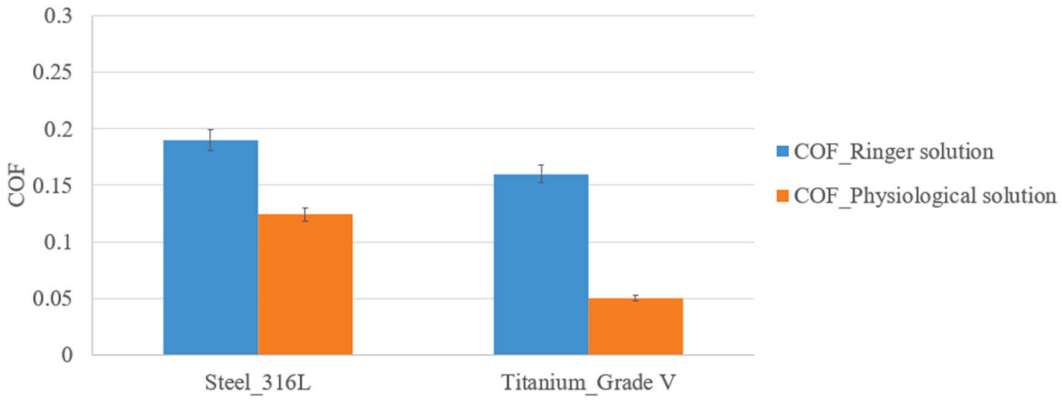

Fig. 7. Mean values of COF of all couplings.

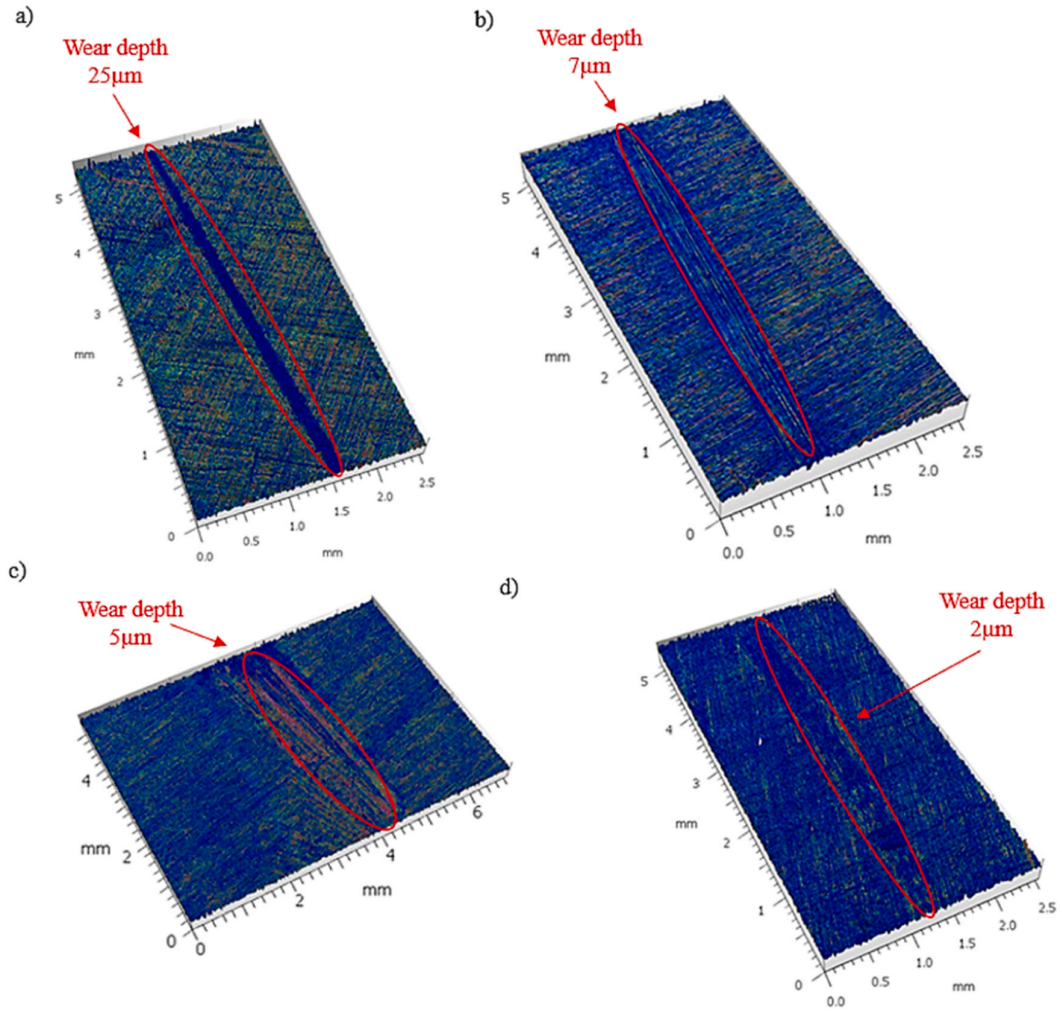

Fig. 8. Wear tracks and depth for Steel 316 L in Ringers' solution (a), physiological solution (b), for Titanium Grade V in Ringer's solution (c) and physiological solution (d).

Watershed algorithm [58] with threshold for merging motifs lower than 5% of profile maximum height (S_z), was performed in order to evaluate the peaks density in the wear track. As expected, increasing the wear the number of peaks becomes higher, and in that sense the stainless steel 316 L provided a greater density (130 and 122 particles/mm^2 for Ringer's and physiological medium) than the Titanium Grade V alloy (103 and 91 particles/mm^2 for Ringer's and physiological medium) with equivalent radius in the range 10–35 µm. In addition, it was found that the mechanical adhesive wear with the presence of directional grooving along the sliding direction was the dominant mechanism as shown in

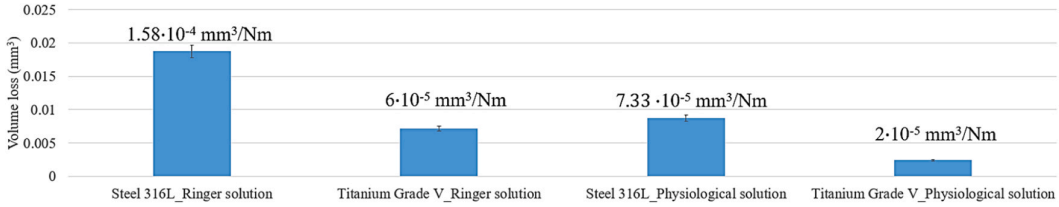

Fig. 12. Total volume loss [mm^3] and wear rate [mm^3/Nm] for stainless steel 316 L and titanium alloys in Ringer and physiological solution.

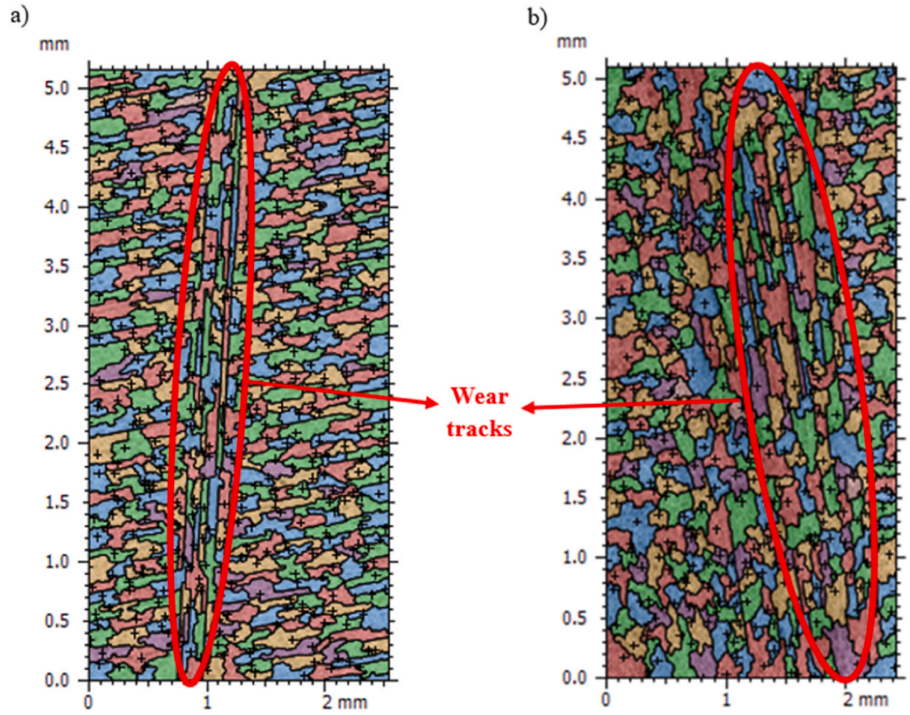

Fig. 9. Example of particle analysis achieved by Watershed algorithm for stainless steel 316 L (a) Titanium Grade V alloy (b) in Ringer's solution.

Fig. 9a-b where the particles in the wear track have the shape of grooves. More precisely, among the four mechanisms of adhesive wear [59], seizure, scoring, scuffing and galling, since the coupling conditions of sliding speed and normal load, the prevalent one was the moderate scoring characterized by evident scratches in the direction of motion and due to the formation of metal-metal contact because of the failure of lubricant fluid, which plays a key role in the biological tribosystems [60]. In addition, pitting corrosion presence was even observed in Steel 316 L and Titanium Grade V (Fig. 10) especially when immersed in Ringer's solution. Indeed, for these samples, the synergistic component, as it will be showed successively, was notable. Moreover the three main texture directions, related to the three biggest peaks, of these samples were reported in Fig. 11. Applying frequency thresholds of 5% and 80% and considering that the secondary peaks at less than 5°of an already detected peak are not taken in account, the directions were for both the materials, in the range 90–115° (Table 6) confirming again the directionality of the wear tracks. Similar results were found out for the same couplings in the physiological medium. The total volume loss was the highest for the stainless steel 316 L in Ringer's solution (0.019 ± 0.003 mm^3) whereas the lowest for Titanium alloy in the physiological solution (0.0024 ± 0.001 mm^3). The other tests provided 0.0072 ± 0.001 mm^3 for Titanium Grade V in Ringer's medium and 0.0088 ± 0.004 mm^3 for stainless steel 316 L in physiological solution. The specific wear rates are respectively, in Ringer's medium, of $1.58\bullet10^{-4}$ and $6\bullet10^{-5}$ mm^3/Nm for steel 316 L and titanium alloy, whereas, in physiological solution, of $7.33\bullet10^{-5}$ and $2\bullet10^{-5}$ mm^3/Nm in concordance with literature outcomes [31,61]. The total wear was, therefore, higher in Ringer's biological fluid than in the other one proving again the impact of chemical solution on tribocorrosion experiments. Moreover, titanium alloy performed better than the Steel 316 L, for both the solutions, having a lower mechanical and consequential tribocorrosive wear [62], although its initial corrosive response was worse. The answer is hidden in its higher hardness but more precisely into the different microstructure of the samples which undergo severe plastic deformation. Indeed, Titanium Grade V owns aluminum and vanadium which stabilize respectively the α and β form providing a greater strength respect to the stainless steel. On the other hand, these two chemical elements are, if spread out, potentially dangerous for our organism: the former may be correlated with osteomalacia (weakness of the bone) [63] while the latter may induce cytotoxic effects and adverse tissue reactions [64]. Hence, the wear debris, considering the biological environment, are of crucial importance because of all the clinical complications likely established. Indeed, the former may be incorporated by macrophages causing their death if the dimensions are large, or not great enough to activate macrophages activity and therefore digested by cells. Moreover, the material loss causes the deterioration and the weaking of the implant-abutment interface and, thus, the performance of the prothesis [65].

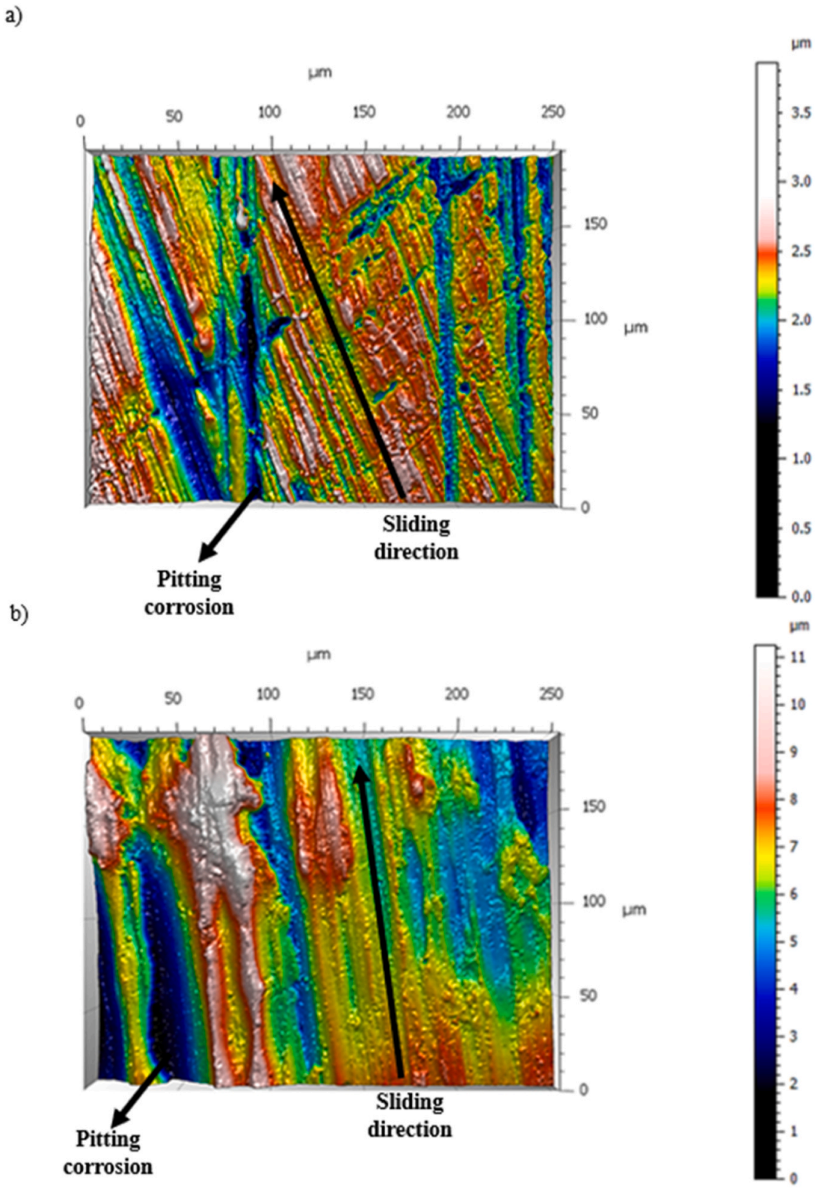

Fig. 10. Extrapolation of wear track of stainless steel 316 L (a) and Titanium Grade V (b) in Ringer's solution. Presence of directional grooving and pitting corrosion.

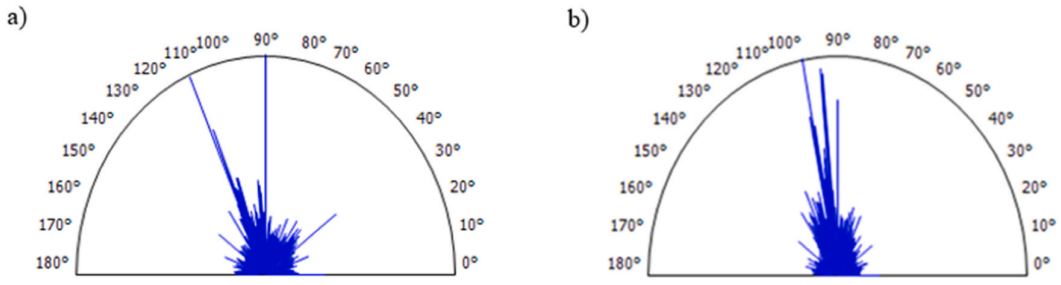

Fig. 11. Texture directions of stainless steel 316 L (a) and Titanium Grade V (b) immersed in Ringer's solution.

Observing the single factors (Fig. 13a-b), estimated in accordance with synergistic approach [66] it is almost evident that the mechanical and synergistic effect, for all the samples, are far higher (Figure13a) than the corrosion part (Fig. 13b) [67] as a consequence of the very low current values [68] which was estimated in the order of 0.01–0.12%, as could be expected taking in account that the samples adopted in the

Table 6
Main directions of stainless steel 316 L and Titanium Grade V immersed in Ringer's solution.

Main directions	Steel 316 L	Titanium Grade V
First direction	90°	101°
Second direction	114°	96°
Third direction	109°	90°

analysis are passive metals [69]. In particular, stainless steel 316 L and Titanium Grade V, in Ringer's medium, have the values of synergy, respectively equals to 77% and 73% of the total wear, but also in the other solution the simultaneous effect of wear and corrosion is not negligible but with lower values, as expected since the diverse chemical nature of the solution, equals respectively to 51% and 20%. This combined action, estimated in the interval 20–80% as stated in literature [70], can be interpreted as both mechanical wear-accelerated corrosion and corrosion-accelerated mechanical wear. In conclusion, the remaining part is attributed to the pure mechanical wear which was principal factor for both the specimens in physiological solution.

Finally, since the synergy impacts on the total wear, as demonstrated also in other works [71,72], an attempt was made to figure out which variable may be correlated with it. In that sense, a direct relationship between friction coefficient and synergy was found, following a linear trend with determination coefficient (R^2) equals to 0.98, as indicated in Fig. 14. It is commonly accepted that friction, considering its physical nature, is connected with mechanical wear [73] via the microcontacts established between asperities [74,75]. This provided the basis for this assumption with the difference that, in this experiment, a corrosive environment is involved, modifying the tribological coupling. Consequently, the COF was related not with the mechanical component but with the synergistic wear, where both corrosion and wear act: the former through chemical reactions and the latter trough the rupture of the contacts induced by the sliding.

3.2. Tribocorrosive current trend

In reference to the conditions introduced in the previous section, the current trend (Fig. 15) was evaluated during a tribocorrosion test, for the four couplings, and compared, in terms of average value with the one obtained via potentiodynamic tests (Fig. 16a-b). After sliding starting, an increase in current, followed by several oscillations, was noted for the samples tested with the exception of Titanium Grade V in physiological solution where it was almost constant. In addition, the effect of motion is more evident for Ringer's medium than the physiological one, where the increase in anodic current value is even present, due to its higher aggressivity. The trends reported in Fig. 15 can be explained considering that the sliding destroys the passive film creating a galvanic coupling between two zones: one active, corresponding to the worn surface, where the protective layer is removed, and one passive, where the latter is still intact [76]. Moreover, the frequency of motion does not provide the sufficient time for a complete repassivation, which was estimated in the interval 25–150 s, subjecting the specimen to tribocorrosive attack of counterpart and solution. In that sense, the sliding promotes the corrosion with values of current even 20 times higher than the ones obtained via potentiodynamic tests where no motion was imposed. Comparing the material response, instead, the titanium alloy, when immersed in Ringer's solution, showed an average value lower than the stainless steel 316 L (1.88±0.09 μA vs 2.4±0.12 μA) owing to the stronger oxide film. Instead, in physiological one, are almost comparable (respectively 0.14±0.07 μA and 0.13±0.06 μA). Overall, the effect of

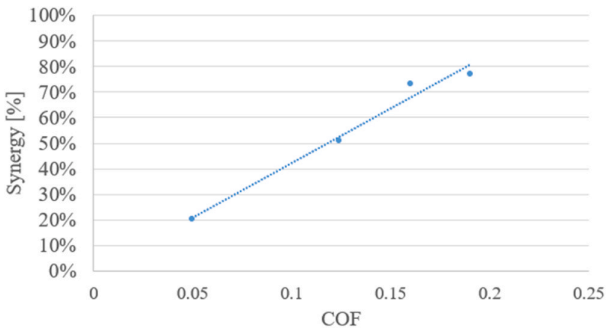

Fig. 14. Synergistic wear-COF relationship: linear trend with determination coefficient $R^2 = 0.98$.

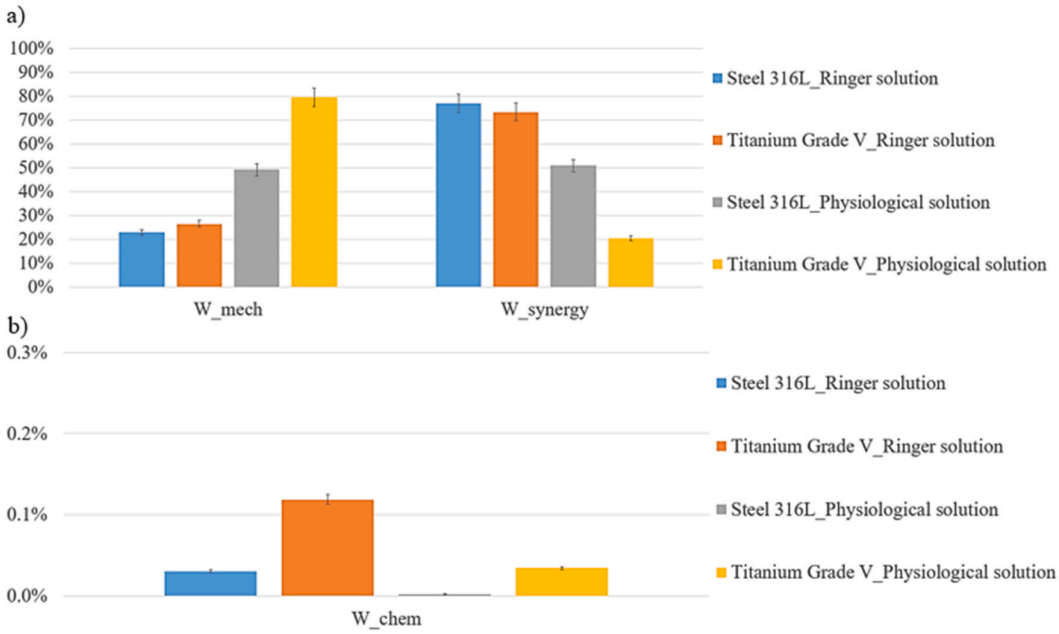

Fig. 13. Synergistic approach. Specific contribution in percentage of mechanical and synergy (a) and chemical (b) wear on total volume loss.

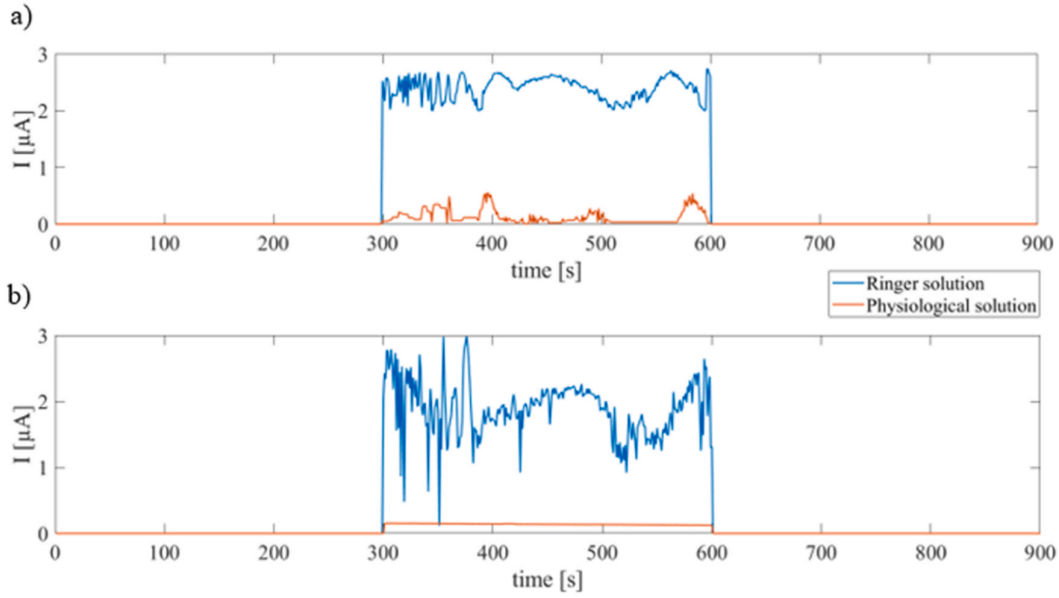

Fig. 15. Current trend during a tribocorrosion test of Steel 316 L (a) and Titanium Grade V (b).

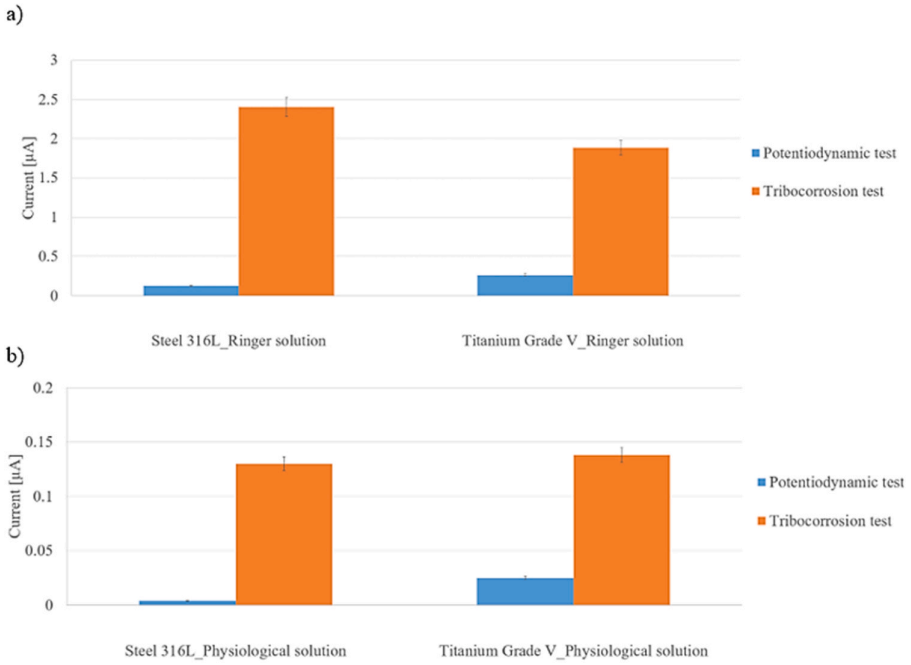

Fig. 16. Current values of all the couplings obtained by potentiodynamic test and during a tribocorrosion experiment for Ringer (a) and physiological (b) solutions.

sliding on corrosion can easily summarized as potential drop and anodic current increase in a such way that the particles removed during the motion are subjected to anodic oxidation before they leave the contact zone. Lastly, a correlation was found also for tribocorrosive current and friction coefficient (Fig. 17) in accordance with a linear trend (R^2 =0.75). This means that when the friction becomes higher more microcontacts are formed and successively destroyed leading to higher currents values [77]. In conclusion, coupling the graphs reported in Figs. 14 and 17 a direct relationship between synergy and tribocorrosive current (R^2 =0.76) is noted which may be adopted for modelling, from an analytical point of view, the synergistic effect. Indeed, at the moment, the latter is evaluated mainly experimentally since a general law has not been provided yet.

4. Conclusions

In this study, two common biomaterials adopted in dental field as stainless steel 316 L and Titanium Grade V, coupled with a Titanium Grade V sphere, were tested in two biological solutions as Ringer's and physiological. Open-circuit potential, potentiostatic, potentiodynamic tests, tribological dry and tribocorrosive experiments were performed allowing to evaluate the OCP during and in absence of sliding, friction

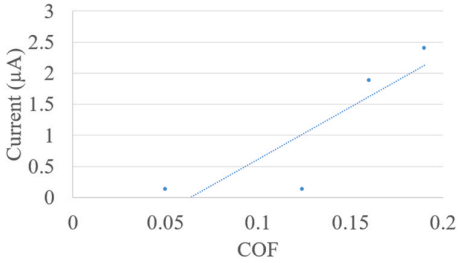

Fig. 17. Tribocorrosive current-COF relationship: linear trend with determination coefficient $R^2 = 0.75$.

coefficient, current trends and total wear. The latter was calculated by synergistic approach and the impact of the single wear component (mechanical, chemical, synergistic) was discussed. In the limitations of this work such as the absence of deeper chemical and topographical characterization of the samples, the manuscript provides interesting outcomes which may be used as future developments for a better comprehension and definition of an ever-changing and interesting scenario as the tribocorrosion one. They can be summarized as follows:

1. The Ringer's medium provided the highest friction coefficients value, tribocorrosive current and material loss. On the other hand, analyzing the material behavior, the Titanium Grade V performed better than stainless steel 316 L in both solutions outlining the best alternative as dental implant material. Nevertheless, the wear debris are absolutely a clinical issue for their effect on human tissues such as inflammations or toxic reactions, reason why new materials or coatings may be added to the bulk material providing increased mechanical and chemical anti-wear properties
2. The total wear is composed mainly of mechanical and synergistic components. In addition, the latter had a significant impact on material loss (20–80%) underling the relevance of the simultaneous action of wear and corrosion which is crucial in the interface between implant and abutment
3. The current values obtained by the potentiodynamic curves were compared with the ones obtained during a tribocorrosion test. An evident increase in current was noted, above all in Ringer's solution. In this light the mechanical wear promotes the corrosion
4. Linear trends between friction coefficient and synergy, and friction with tribocorrosive current, were found (determination coefficient, R^2 =0.98 and 0.75 respectively) confirming a direct relationship between synergy and tribocorrosive current (R^2 =0.76) which may be involved in future analytical models

Overall, tribocorrosion is a multivariable phenomenon, including several factors, from different engineering areas. The topic is, with no doubt, current and, at the same time, needing of other experimental tests where diverse setup conditions, varying the chemical composition of the solution or the specimen material for example, may be adopted with aim of strengthening the current scientific knowledge. In that sense, other approaches could be useful as numerical analysis, especially finite element method which is a very common tool in biomedical dental applications [78], as much as clinical trials, investigating the tribocorrosive behavior of the samples in a more complex biological environment, involving also the presence of bacteria.

Declaration of Competing Interest

The authors declare that they have no known competing financial interests or personal relationships that could have appeared to influence the work reported in this paper.

Data availability

Data will be made available on request.

Acknowledgements

This research was supported by MIUR PRIN 2017 BIONIC.

References

[1] Fedrizzi L, Valentinelli L, Rossi S, Segna S. Tribocorrosion behaviour of HVOF cermet coatings. Corros Sci 2007;49(7):2781–99.
[2] Wood RJK. Marine wear and tribocorrosion. Wear 2017;376–377(Part B):893–910.
[3] Maleque MA, Cetin SY, Hassan M, Sulaiman MH, Rosli AH. A systematic review on corrosive-wear of automotive components. J Tribol 2022;35:33–49.
[4] Diomidis N, Celis JP, Ponthiaux P, Wenger F. Tribocorrosion of stainless steel in sulfuric acid: Identification of corrosion–wear components and effect of contact area. Wear 2010;269:93–103.
[5] Ruggiero A, Zhang H. Biotribology and biotribocorrosion properties of implantable biomaterials. Front Mech Eng 2020;6:17.
[6] Mathew MT, Runa MJ, Laurent M, Jacobs JJ, Rocha LA, Wimmer MA. Tribocorrosion behavior of CoCrMo alloy for hip prosthesis as a function of loads: A comparison between two testing systems. Wear 2011;217:1210–9.
[7] De Stefano M, Aliberti SM, Ruggiero A. Bio)Tribocorrosion in dental implants: principles and techniques of investigation. Appl Sci 2022;12:7421.
[8] Alves SA, Bayón R, Viteri VD, Garcia MP, Igartua A, Fernandes MH, Rocha LA. Tribocorrosion behavior of calcium- and phosphorous-enriched titanium oxide films and study of osteoblast interactions for dental implants. J Bio- Tribo-Corros 2015;1:23.
[9] Landolt D, Mischler S, Stemp M. Electrochemical methods in tribocorrosion: a critical appraisal. Electrochim Acta 2001;46:3913–29.
[10] Diomidis N, Celis JP, Ponthiaux P, Wenger F. A methodology for the assessment of the tribocorrosion of passivating metallic materials. Lubr Sci 2009;21:53–67.
[11] Souza JCM, Henriques M, Teughels W, Ponthiaux P, Celis JP, Rocha LA. Wear and corrosion interactions on titanium in oral environment: literature review. J Bio-Tribo-Corros 2015;1(2):13.
[12] Guo Z, Pang X, Yan Y, Gao K, Volinsky A, Zhang TY. CoCrMo alloy for orthopedic implant application enhanced corrosion and tribocorrosion properties by nitrogen ion implantation. Appl Surf Sci 2015;347:23–34.
[13] Kheder W, Kawas S, Khalaf K, Samsudin AR. Impact of tribocorrosion and titanium particles release on dental implant complications — A narrative review. Jpn Dent Sci Rev 2021;57:182–9.
[14] Veeman D, Katiyar JK, Ruggiero A. Tribo-mechanical performance of brake composite material: a comprehensive review. Tribology - Materials. Surf Interfaces 2023:1–24.
[15] Malik A, Rouf S, Haq MU, Raina A, Puerta AP, Sagbas B, Ruggiero A. Tribo-corrosive behavior of additive manufactured parts for orthopaedic applications. J Orthop 2022;34:49–60.
[16] Wood RJK, Wharton JA. Coatings for tribocorrosion protection. Tribocorrosion Passiv Met Coat: Woodhead Publ Ser Met Surf Eng 2011:296–333.
[17] Azzi M, Paquette M, Szpunar J, Klemberg-Sapieha J, Martinu L. Tribocorrosion behaviour of DLC-coated 316L stainless steel. Wear 2009;267:860–6.
[18] Alonso-Falleiros N, Hakim A, Wolynec S. Comparison between potentiodynamic and potentiostatic tests for pitting potential measurement of duplex stainless steels. Corrosion 1999;55(5):443–8.
[19] Mischler S. Triboelectrochemical techniques and interpretation methods in tribocorrosion: A comparative evaluation. Tribology Int 2008;41:573–83.
[20] Ponthiaux P, Wenger F, Drees D, Celis JP. Electrochemical techniques for studying tribocorrosion processes. Wear 2004;256:459–68.
[21] Cao S, Mischler S. Modeling tribocorrosion of passive metals – A review. Curr Opin Solid State Mater Sci 2018;22(4):127–41.
[22] Zhang BB, Wang JZ, Zhang Y, Han GF, Yan FY. Tribocorrosion behavior of 410SS in artificial seawater: effect of applied potential. Mater Corros 2017;68(3):295–305.
[23] Zhang G, Cui W, Peng X, Pu J, Li J, Jin Z. Effect of angular mismatch on tribocorrosion at taper-trunnion junction using a finite element model considering mechanical and chemical wear. Tribology Int 2023;184:108477.
[24] Dalmau A, Muñoz A, Mischler S. Current and friction transients during tribocorrosion of a biomedical titanium alloy sliding against zirconia. Wear 2023; 524–525:204821.
[25] Wang Z, Huang W, Li Y, He H, Zhou Y, Zheng Z. Tribocorrosion behaviour of a biomedical Ti-25Nb-3Mo-3Zr-2Sn alloy in Ringer's solution. Mater Sci Eng: C 2017;76:1094–102.
[26] Shivaram MJ, Arya SB, Nayak J, Panigrahi B. Tribocorrosion behaviour of biomedical porous Ti–20Nb–5Ag alloy in simulated body fluid. J Bio- Tribo-Corros 2021;7(59).
[27] Royhman D, Yuan JC, Shokuhfar T, Takoudis C, Sukotjo C, Mathew MT. Tribocorrosive behaviour of commonly used temporomandibular implants in a synovial fluid-like environment: Ti–6Al–4V and CoCrMo. J Phys D: Appl Phys 2013;46(40):404002.
[28] Sivakumar B, Pathak LC, Singh R. Role of surface roughness on corrosion and fretting corrosion behaviour of commercially pure titanium in Ringer's solution for bio-implant application. Appl Surf Sci 2017;401:385–98.

[29] Neto MQ, Rainforth WM. Effect of potential and microstructure on the tribocorrosion behaviour of beta and near beta Ti alloys II. J Bio- Tribo-Corros 2021;7:141.
[30] Wang Z, Yan Y, Su Y, Qiao L. Effect of proteins on the surface microstructure evolution of a CoCrMo alloy in bio-tribocorrosion processes. Colloids Surf B: Biointerfaces 2016;145:176–84.
[31] Carquigny S, Takadoum J, Ivanescu S. Corrosion and tribocorrosion study of 316L steel, Ti–6Al–4V andTi–10Zr–10Nb–5Ta. Tribology-Mater, Surf Interfaces 2019;13 (2):112–9.
[32] Yan Y, Neville A, Dowson D. Biotribocorrosion of CoCrMo orthopaedic implant materials—Assessing the formation and effect of the biofilm. Tribology Int 2007;40 (10–12):1492–9.
[33] Axente ER, Benea L, Bogatu N, Celis JP. Susceptibility to tribocorrosion degradation of 304 L stainless steel from dental structures in biological solution. Tribology Int 2022;174:107769.
[34] Yazdi R, Ghasemi HM, Abedini M, Wang C, Neville A. Tribocorrosion behaviour of Ti6Al4V under various normal loads in phosphate buffered saline solution. Trans Nonferrous Met Soc China 2020;30(5):1300–14.
[35] Landolt D. Electrochemical and materials aspects of tribocorrosion systems. J Phys D: Appl Phys 2006;39:3121–7.
[36] Khan AS, Awais M. Low-Cost Deposition of Antibacterial Ion-Substituted Hydroxyapatite Coatings onto 316L Stainless Steel for Biomedical and Dental Applications. Coatings 2020;10(9):880.
[37] Velasco-Ortega E, Jos A, Cameán AM, Pato-Mourelo J, Segura-Egea JJ. In vitro evaluation of cytotoxicity and genotoxicity of a commercial titanium alloy for dental implantology. Mutat Res: Genet Toxicol Environ Mutagen 2010;702(1): 17–23.
[38] De Stefano M, Lanza A, Faia E, Ruggiero A. A novel ultrashort dental implant design for the reduction of the bone stress/strain: A comparative numerical investigation. Biomed Eng Adv 2023;5:100077.
[39] Chen J, Mraied S, Cai W. Determining tribocorrosion rate and wear-corrosion synergy of bulk and thin film aluminum alloys. J Vis Exp 2018;139:58235.
[40] Alfaro MF, Rossman PK, Marques ISV, Dube A, Takoudis C, Shokuhfar T, Mathew MT, Sukotjo C. Interface damage in titanium dental implant due to tribocorrosion: the role of mastication frequencies. J Bio- Tribo-Corros 2019;5(4): 81.
[41] Ohe CBd Johnsen R, Espallargas N. Modeling the multi-degradation mechanisms of combined tribocorrosion interacting with static and cyclic loaded surfaces of passive metals exposed to seawater. Wear 2010;269(7–8):607–16.
[42] Mehkri S, Abishek NR, Sumanth KS, Rekha N. Study of the Tribocorrosion occurring at the implant and implant alloy Interface: Dental implant materials. Mater Today: Proc 2021;44:157–65.
[43] Barril S, Debaud N, Mischler S, Landolt D. A tribo-electrochemical apparatus for in vitro investigation of fretting–corrosion of metallic implant materials. Wear 2002; 252(9–10):744–54.
[44] Chen J, Zhang Q, Li QA, Fu SL, Wang JZ. Corrosion and tribocorrosion behaviors of AISI 316 stainless steel and Ti6Al4V alloys in artificial seawater. Trans Nonferrous Met Soc China 2014;24(4):1022–31.
[45] Brownlie F, Hodgkiess T, Pearson A, Galloway A. Electrochemical Evaluation of the Effect of Different NaCl Concentrations on Low Alloy- and Stainless Steels under Corrosion and Erosion-Corrosion Conditions. Corros Mater Degrad 2022;3(1): 101–26.
[46] Shahba RM, Ghannem WA, El-Shenawy AS, Ahmed ASI, Tantawy SM. Corrosion and Inhibition of Ti-6Al-4V Alloy in NaCl Solution. Int J Electrochem Sci 2011;6: 5499–509.
[47] Golvano I, Garcia I, Conde A, Tato W, Aginagalde A. Influence of fluoride content and pH on corrosion and tribocorrosion behaviour of Ti13Nb13Zr alloy in oral environment. J Mech Behav Biomed Mater 2015;49:186–96.
[48] Zhang Y, Yin X, Yan Y, Wanga J, Yan F. Tribocorrosion behaviors of 304SS: Effect of solution pH. RSC Adv 2015;5(23).
[49] Brończyk A, Kowalewski P, Samoraj M. Tribocorrosion behaviour of Ti6Al4V and AISI 316L in simulated normal and inflammatory conditions. Wear 2019:434–5. 202966.
[50] Zhang Y, Yin XY, Yan FY. Tribocorrosion behaviour of type S31254 steel in seawater: Identification of corrosion–wear components and effect of potential. Mater Chem Phys 2016;179:273–81.
[51] Ji X, Luo C, Jin J, Zhang Y, Sun Y, Fu L. Tribocorrosion performance of 316L stainless steel enhanced by laser clad 2-layer coating using Fe-based amorphous powder. J Mater Res Technol 2022;17:612–21.
[52] Vieira AC, Ribeiro AR, Rocha LA, Celis JP. Influence of pH and corrosion inhibitors on the tribocorrosion of titanium in artificial saliva. Wear 2006;261:994–1001.
[53] Mathew MT, Uth T, Hallab NJ, Pourzal R, Fischer A, Wimmer MA. Construction of a tribocorrosion test apparatus for the hip joint: Validation, test methodology and analysis. Wear 2011;271(9–10):2651–9.
[54] Barona-Osorio GM, Teran LA, Rodríguez SA, Coronado JJ. On the Tribocorrosion Behavior of Fe-Mn-Al-C Alloys in Ringer's Solution. Metals 2022;12(8):1339.
[55] Chen J, Wang J, Chen B, Yan F. Tribocorrosion Behaviors of Inconel 625 Alloy Sliding against 316 Steel in Seawater. Tribology Trans 2011;54:514–22.
[56] Landolt D, Mischler S, Stemp M, Barril S. Third body effects and material fluxes in tribocorrosion systems involving a sliding contact. Wear 2004;256(5):517–24.
[57] Priya R, Mallika C, Mudali UK. Wear and tribocorrosion behaviour of 304L SS, Zr-702, Zircaloy-4 and Ti-grade2. Wear 2014;310(1–2):90–100.
[58] Ruggiero A, De Stefano M. On the biotribological surfaces of dental implants: investigation in the framework of osseointegration. Biotribology 2023;35–36: 100254.
[59] Markov D, Kelly D. Mechanisms of adhesion-initiated catastrophic wear: pure sliding. Wear 2000;239:189–210.
[60] Ruggiero A. Milestones in natural lubrication of synovial joints. Front Mech Eng 2020;6:52.
[61] Namus R, Nutter J, Qi J, Rainforth WM. Sliding speed influence on the tribo-corrosion behaviour of Ti6Al4V alloy in simulated body fluid. Tribology Int 2021; 160:107023.
[62] Alberta LA, Vishnu J, Douest Y, Perrin K, Trunfio-Sfarghiu AM, Courtois N, Gebert A, Ter-Ovanessian B, Calin M. Tribocorrosion behavior of β-type Ti-Nb-Ga alloys in a physiological solution. Tribology Int 2023;181:108325.
[63] Boyce BF, Elder HY, Elliot HL, Fogelman I, Fell GS, Junor BJ, Beastall G, Boyle IT. Hypercalcemic Osteomalacia Due To Aluminium Toxicity. Lancet 1982;320(8306): 1009–13.
[64] Evangelou AM. Vanadium in cancer treatment. Crit Rev Oncol/Hematol 2002;42 (3):249–65.
[65] Wang Z, Zhou Y, Wang H, Li Y, Huang W. Tribocorrosion behavior of Ti-30Zr alloy for dental implants. Mater Lett 2018;218:190–2.
[66] Kowalski M, Stachowiak A. Tribocorrosion Performance of Cr/CrN Hybrid Layer as a Coating for Machine Components Used in a Chloride Ions Environment. Coatings 2021;11:242.
[67] Ferreira DF, Almeida SMA, Soares RB, Juliani L, Bracarense AQ, Lins VDF, Junqueira RM. Synergism between mechanical wear and corrosion on tribocorrosion of a titanium alloy in a Ringer solution. J Mater Res Technol 2019;8 (2):1593–600.
[68] Ji X, Luo C, Sun Y, Zhao J. Corrosive wear of multi-layer Fe-based coatings laser cladded from amorphous powders. Wear 2019;438–439:203113.
[69] Namus R, Rainforth WM. The influence of cathodic potentials on the surface oxide layer status and tribocorrosion behaviour of Ti6Al4V and CoCrMo alloys in simulated body fluid. Biotribology 2022;30:100212.
[70] Henry P, Takadoum J, Berçot P. Tribocorrosion of 316L stainless steel and TA6V4 alloy in H2SO4 media. Corros Sci 2009;51(6):1308–14.
[71] Naghibi SA, Raeissi K, Fathi MH. Corrosion and tribocorrosion behavior of Ti/TiN PVD coating on 316L stainless steel substrate in Ringer's solution. Mater Chem Phys 2014;148(3):614–23.
[72] Tekin KC, Malayoglu U. Assessing the tribocorrosion performance of three different nickel-based superalloys. Tribology Lett 2009;37:563–72.
[73] Kato K. Wear in relation to friction — a review. Wear 2000;241(2):151–7.
[74] Ruggiero A, De Stefano M. Evaluation of the real contact area of rough surfaces by using a finite element model. Advances in Italian Mechanism Science IFToMM ITALY 2020 Mechanisms and Machine Science, 91. Cham: Springer,; 2020.
[75] De Stefano M, Ruggiero A. Real contact area and friction. Industrial Tribology. CRC Press,; 2022.
[76] Berradja A, Bratu F, Benea L, Willems G, Celis JP. Effect of sliding wear on tribocorrosion behaviour of stainless. Wear 2006;261:987–93.
[77] Stemp M, Mischler S, Landolt D. The effect of mechanical and electrochemical parameters on the tribocorrosion rate of stainless steel in sulphuric acid. Wear 2003;255:466–75.
[78] Trivedi S. Finite element analysis: a boon to dentistry. J Oral Biol Craniofacial Res 2014;4(3):200–3.